Electronic structure and metamagnetic transition of interstitially doped $LaSiFe_{12}$

Z. Gercsi,[1,2] K.G. Sandeman,[2,3,4] and A. Fujita[5]

[1] *CRANN and School of Physics, Trinity College Dublin, Dublin 2, Ireland*
[2] *Dept. of Physics, Blackett Laboratory, Imperial College London, London SW7 2AZ, United Kingdom*
[3] *Dept. of Physics, Brooklyn College, CUNY, 2900 Bedford Avenue, Brooklyn, New York 11210, USA*
[4] *The Graduate Center, CUNY, 365 Fifth Avenue, New York, New York 10016, USA*
[5] *Green-Innovative Magnetic Material Research Center, National Institute of Advanced Industrial Science and Technology Anagahora 2266-98, Simosidami, Nagoya 463-8560, Japan*

arXiv:1407.7975v1 [cond-mat.mtrl-sci] 30 Jul 2014

We present a systematic investigation of the effect of H, B, C, and N interstitials on the electronic, lattice and magnetic properties of $La(Fe,Si)_{13}$ using density functional theory. The parent $LaSiFe_{12}$ alloy has a shallow, double-well free energy function that is the basis of first order itinerant electron metamagnetism. On increasing the dopant concentration, the resulting lattice expansion causes an initial increase in magnetisation for all interstitials that is only maintained at higher levels of doping in the case of hydrogen. Strong *s-p* band hybridisation occurs at high B,C and N concentrations. We thus find that the electronic effects of hydrogen doping are much less pronounced than those of other interstitials, and result in the double-well structure of the free energy function being least sensitive to the amount of hydrogen. This microscopic picture accounts for the change in the metamagnetic transition from first order to second order on doping with B,C, and N interstitials, as observed experimentally.

PACS numbers: 71.20.-b, 75.30.Kz, 75.30.Sg

I. INTRODUCTION

The magnetocaloric effect (MCE) is the temperature change of a substance subjected to a change in applied magnetic field. The discovery of the effect can be attributed to Weiss and Piccard's observation of the magnetization of nickel close to its Curie point in 1917,[1]after a recent re-examination of the original literature by Smith.[2] The adiabatic demagnetization of paramagnetic salts was shown by Giauque and MacDougall in 1933[3] following initial proposals by both Debye and Giauque in the previous decade.[4,5] The study of room temperature MCEs associated with a magnetic phase transition was revived in 1997 by Pecharsky and Gschneidner who observed a 'giant' entropy change of $\sim$14 $JK^{-1}kg^{-1}$ in a 0-2 Tesla field change in $Gd_5Si_2Ge_2$.[6] While experiments up to that point had postulated the possibility of room temperature refrigeration using, for example, a second order Curie transition such as that found in Gd,[7] it was the effects associated with the first order transition seen in $Gd_5Si_2Ge_2$ that initiated widespread research interest in the MCE. Today, a large set of magnetic materials show 'large' or 'giant' magnetocaloric effects.[8] However, a good refrigerant material also needs to fulfil auxiliary requirements such as tuneable thermal conductivity, durability and elemental abundance and so the number of material systems that are close to commercialisation is relatively small. This situation provides motivation for the use of theoretical models that may aid the understanding and prediction of magnetocaloric effects.

Density functional theory (DFT) is a valuable tool with which to describe the changes in matter at the electronic level that may lead to a large MCE. Elemental Gd has a ferromagnetic (FM) ordering temperature around room temperature that makes it an ideal candidate magnetocaloric material. DFT calculations based on thermally induced spin fluctuations in a disordered local moment picture showed that the magnetic order in Gd is linked to the c/a ratio and atomic unit cell volume.[9] Such magneto-elastic coupling is useful for generating a large MCE. However, the cost of heavy rare-earth Gd inhibits its use in everyday applications as refrigerant. In $Gd_5(Si_2Ge_2)$, DFT calculations indicated breaking and reforming of Si-Ge bonds between layers within the unit cell, affecting both the location of the Fermi level and the effective magnetic exchange coupling, increasing the latter to the level where a first order magneto-structural transition is observed.[6]

Manganites and manganese silicides have also been the subject of DFT studies. In manganites, the broad variety of crystallographic, magnetic and electronic phases are attributed to the strong interplay between spin, charge, orbital and lattice degrees of freedom that often couples to external magnetic fields and results in measurable MCE. For a qualitative description of these correlated physical quantities, state-of-the-art hybrid exchange density functionals such can be applied.[10] In the case of manganese based metallic silicides, ground state and finite temperature DFT models have been used to model and predict new Mn-based metamagnets.[11–13] Those calculations used accurate structural data obtained from high resolution neutron diffraction on CoMnSi, a noncollinear antiferromagnet (AFM) that exhibits giant magneto-elastic coupling.[14]

Experimentally, the most intensively studied MCE materials are based on either Fe_2P or $La(Fe,Si)_{13}$. Both have been the subject of some modelling studies. In Fe_2P, iron has two inequivalent crystallographic sites and the low moment site ($3f$) has a metamagnetic transition[15] at the Curie temperature, 212 K. The Curie point can be tuned

through room temperature by partial replacement of Fe by Mn as well as P by, for example, Si.[16] The so-called mixed magnetism of this material has been investigated by a number of DFT studies that have identified the mechanism of magneto-elastic coupling and the change of electron density across the Curie transition.[16–20]

In this article, we perform a DFT study of compounds based on $LaFe_{13-x}M_x$ (M=Si, Al), a cubic $NaZn_{13}$-type material which was first synthesized by Kripyakevich et al.[21] To date, much of the compositional tuning that is used to adjust the magnetocaloric effect and its temperature range is the result of empirical work rather than theory-led prediction.

$LaFe_{13-x}M_x$ exhibits a large MCE associated with a paramagnetic to ferromagnetic transition on cooling at a temperature, T_C, between 180 and 250 K. A magnetic field-dependent itinerant-electron metamagnetic (IEM) transition above T_C, can be shifted towards room temperature by Si addition. However, on increasing the Si content above $x > 1.8$, a change in the nature of the FM phase transition from first-order to second-order takes place that results in a considerable reduction of the useful MCE. A first-principles calculation by Wang et al.[24] indicated that hybridization between the Fe-d and Si-p states is linked to the reduction of Fe magnetic moment as well as to the smearing of the first-order type transition for alloys with high Si-content.

The partial replacement of the transition metal element Fe by Co or Mn has been explored in an attempt to preserve the first order nature of the transition around the Curie temperature, T_C, although both elements cause significant weakening of the field-induced IEM transition[25]. Similarly, interstitial doping of s-block or p-block elements was also pursued experimentally in order to raise the IEM to room temperature. These empirical studies found that the preparation of single phase compositions is limited to low interstitial concentrations and that only hydrogen is capable of the increase of magnetic transition to room temperature without the diminution of useful isothermal entropy change.[23] Theoretical calculations by Kuz'min and Richter[26] on $LaFe_{12}Si$, without interstitial substitution, found that the free energy, as a function of magnetization ($F(M)$) has several shallow minima and maxima, to which they attributed the reduced hysteresis and improved magnetocaloric performance of $La(Fe,Si)_{13}$. Recently, Fujita and Yako[27] extended this approach and further detailed the dependence of such an energy plot on both the lattice size and the degree of Fe/Si substitution.

We note that no systematic investigation of the effect of interstitial s-block or p-block elements on the electronic, lattice and magnetic properties of $La(Fe,Si)_{13}$ has been carried out to date. The work presented here, using a theoretical approach based on DFT, attempts to describe the effect of the size of four different dopants and their valence electrons to understand how interstitials can influence the magnetocaloric performance of these alloys. We describe our theoretical methods in section II before presenting our results and discussion in section III. Conclusions are drawn in section IV.

II. METHODS

A. Computational models used

Our computational approach is divided into two, complementary parts. In the first part, we investigate the effect of interstitial doping on the equilibrium unit cell volume using the projector augmented wave (PAW) method[28] as implemented in the Vienna ab-initio simulation package (VASP). The VASP code with Perdew-Burke-Ernzerhof (PBE) parameterization[29] is employed, where site-based magnetic moments were calculated using the Vosko-Wilk-Nusair interpolation[30] within the general gradient approximation (GGA) for the exchange-correlation potential.

$La(Fe,Si)_{13}$ has 8 formula units per conventional cell. The La atoms occupy the 8a sites ($\frac{1}{4},\frac{1}{4},\frac{1}{4}$), while diffraction studies show that Fe and Si atoms can occupy both 8b (000) and the 96i (0yz) crystallographic positions.[31–34] In order to keep the computational requirements at a feasible level, we follow the approach previously adopted by Kuz'min and Richter,[26] limiting our investigations to an atomically ordered version of $LaSiFe_{12}Z_x$, where the 8b sites are occupied solely by silicon whilst iron is located exclusively on the 96i sites. In such a case, the cell that forms the basis of the calculations contains 2 La, 26 Fe and 2 Si atoms. Furthermore, interstitial elements (Z) H, B, C, and N were considered to occupy the 24d crystallographic site only. Using this model, we may vary the concentration of interstitials, x_Z in a step size of 0.5 from $x = 0$ to 3 in $LaSiFe_{12}Z_x$.

Full structural relaxation was carried out for both collinear ferromagnetic (FM) and non-magnetic (NM) states in the case of parent $LaFe_{12}Si$ alloy, while only the lattice parameter a was relaxed (without relaxation of the internal atomic positions) for the materials doped with s- or p-block interstitials. A $7 \times 7 \times 7$ k-point grid was used to discretize the first Brillouin zone and the energy convergence criterion was set to 5×10^{-7} eV during the energy minimization process. The spin-orbit interaction was turned off during the calculations. Finally, data presented in Fig. 2 was calculated on a dense $19 \times 19 \times 19$ grid of k-points for high accuracy.

In the second part of this study, we have taken a fixed spin moment (FSM) approach within the tight-binding theorem using linear muffin tin orbitals (TB-LMTO) as implemented in Stuttgart TB-LMTO code.[35–37] This method requires carefully adjusted overlapping Wigner-Seitz (WS) atomic spheres included in the calculations to complete the basis and to provide an accurate description of the electron density throughout the entire unit cell. Consequently, the structural parameters of the relaxed lattice are inherently dependent on the volume occupied by the WS spheres and/or empty spheres. For

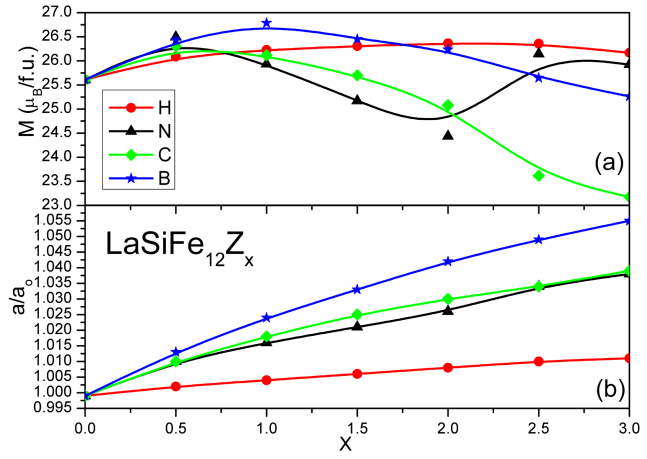

Figure 1: Magnetic moment/formula unit (a) and relative lattice expansion ($\frac{a}{a_0}$) (b) as a function of dopant concentration in $LaSiFe_{12}Z_x$. The lattice parameter a_0 corresponds to the fully relaxed, interstitials free FM structure.

this reason, we used VASP code (see above) for relaxation. Nevertheless, the TB-LMTO approach allows us to evaluate the total energy difference between FM and NM states, $\Delta F(M)$ as a function of fixed spin moment M as well as the corresponding density of states (DOS) and band dispersions. H, B, C, and N atoms were considered to fully occupy the 24*d* crystallographic site, $LaSiFe_{12}Z_3$, for the study. A dense mesh with 48×48×48 k-points (for the DOS calculations) or with 12×12×12 k-points (for the FSM calculations) was used.

III. RESULTS AND DISSCUSSION

A. Effect of dopants on the lattice expansion and magnetic properties

Fig. 1 shows the calculated lattice parameter in the FM state in $LaSiFe_{12}Z_x$ as a function of interstitial doping. Our calculations obtain a relaxed structure that differs by only about 0.1% from the experimentally reported value. This remarkable agreement validates our choice of exchange correlation, GGA. The lattice expansion increases monotonically with dopant concentration at a rate that depends strongly on the size of the interstitial element. The empirical atomic radius of hydrogen (25 pm) is much smaller than that of the boron (85 pm), carbon (70 pm), or nitrogen (65 pm). The trend in calculated lattice expansion in Fig. 1 correlates well with the relative atomic size of the interstitial, showing the predominant influence of the latter on the size of the unit cell. At full doping ($x = 3$), we here find a relative lattice expansion of 0.4% for hydrogen and a considerably higher value of 1.7% for carbon**,** which match with the experimental values H and C, respectively.[38,39] The values of $\frac{\triangle a}{a}$ are 1.8% and 1.25% for Z=B and N respectively at full doping, but these are yet to be confirmed experimentally.

There are only limited experimental data available on the relative effects of lattice expansion of the dopants studied here, particularly as full occupation of the 24*d* site ($x = 3$) by any of the dopants has not been achieved in practice. In terms of valence electron number, however, a different sequence exists: $H(s^1) = B(p^1) < C(p^2) < N(p^3)$. A closer look at Fig. 1 reveals a non-monotonic behaviour in the lattice expansion as a function of doping, especially in the case of nitrogen. Indeed, additional charges significantly alter the electronic structure (apart from H) in ways that go beyond the simple picture of chemical pressure effects, as we discuss later. The contribution of additional valence electrons is also reflected in the calculated magnetic moment (M). M rises initially (Fig. 1, top) for each dopant but a monotonic increase up to $x = 2.5$ is only seen in the case of hydrogen. These observations imply a mechanism for hybrid band formation and band broadening for any dopant with a larger atomic radius than that of hydrogen.

In order to depict the changes in the electronic structure that are brought about by the interstitial elements, we next examine the partial electronic density of states (PDOS). Fig. 2 shows the PDOS of the parent alloy together with the fully hydrogenated and fully nitrogenated materials ($x = 3$). In the parent alloy (bottom), the PDOS is dominated by Fe (red line) around the Fermi level (E_F) with typical spin-split states. The spin-up (↑) states are mostly occupied, while the unoccupied states are dominated by spin-down (↓) states separated by about 2.5eV in energy. Furthermore, the filled bands at the lower end of energy range (-9.5 eV) relate mostly to silicon 3*s* states which are overlapped with *p*-states of both La and Fe. A large energy gap appears from -9.5 eV up to about -6.5eV, where a high population of 3*p* states of Si (black) is located (-6.5 to -4.5 eV). In this latter energy range, there is negligible contribution from Fe *d*-states. Most of the aforementioned features in the electronic structure are preserved in fully hydrogenated $LaSiFe_{12}H_3$ (middle of Fig. 2). The main difference in the PDOS compared to the parent alloy is the development of additional states in the gap around -7.5 eV related to the hydrogen interstitials. Small additional peaks also appear around -5 eV, where they overlap with the *p* states of Si.

In strong contrast to hydrogenation, fully nitrogenated $LaSiFe_{12}N_3$ exhibits a large overlap of N *p* states with Fe *d* states in the -7.5 to -4 eV energy interval (top of Fig. 2). These peaks indicate $p-d$ hybridization, and as a result, increased covalency in bond formation. Another important consequence of nitrogenation is the appearance of states in the vicinity of the Fermi level. The existence of a "double peak" feature just below and above E_F for $LaSiFe_{12}$, created by Fe *d* states in the minority DOS, is altered only a little by hydrogenation. On the other hand, nitrogenation fills this valley at E_F, which results in the strong alteration of the magnetic properties and ultimately leads to the disappearance of IEM transition.

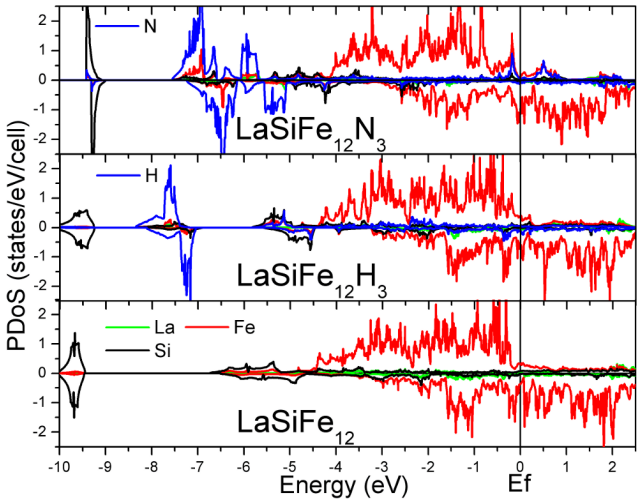

Figure 2: Partial density of states (PDOS) of the parent $LaSiFe_{12}$ alloy (bottom) in comparison with $LaSiFe_{12}H_3$ (middle) and $LaSiFe_{12}N_3$ (top).

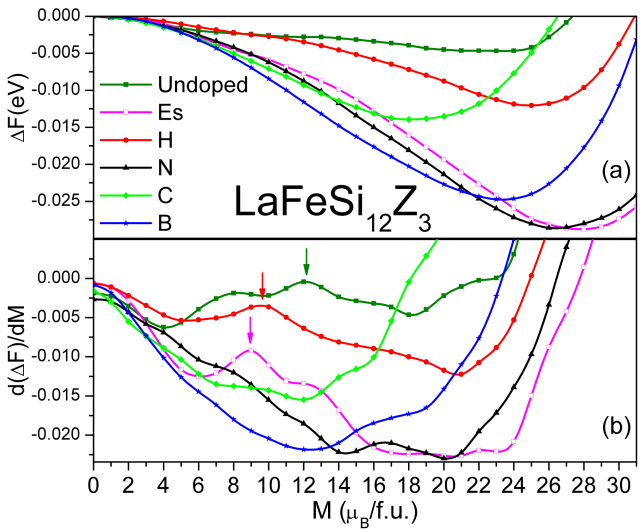

Figure 3: Free energy of the FM state (relative to the free energy of the non-magnetic state) as a function of magnetization M, calculated by the fixed spin method (FSM) for $LaSiFe_{12}Z$ and for $LaSiFe_{12}Z_3$, (Z = H, N, B, empty sphere (Es)). (b) The derivative, $d(\Delta F)/dM$. Local minima in the free energy occur where $d(\Delta F)/dM = 0$.

We address the latter behavior in detail in the next section.

B. The free energy landscape

We now turn our interest to the results of our second computational approach, fixed spin moment calculations using TB-LMTO. Our aim is to visualize the energy difference between FM and NM states in the parent alloy and the doped materials. The purpose of our analysis is to identify the main factors that lead to the field-induced isothermal entropy change of $LaSiFe_{12}Z_3$ around the magnetic transition being lower than that of $LaSiFe_{12}$, as found experimentally for interstitials other than hydrogen.

Fig. 3 compares the free energy curves $F(M)$ calculated by the FSM method for $LaSiFe_{12}Z_3$, where Z = H, N, B and empty sphere (Es), respectively, together with those of the parent alloy. For direct comparison, we set the non-magnetic energy state as F(0) for each individual composition. Fig. 3(a) shows that the parent $LaSiFe_{12}$ has a very shallow magnetic energy landscape, in accordance with the predictions by Kuz'min and Richter, who used the full-potential local-orbital (FPLO) method.[26] They noted the advantage of such a potential energy landscape in permitting a low hysteresis, first order metamagnetic transition (IEM). The main difference in our calculation of the parent compound is that we find only two minima rather than the multiple minima that were predicted in their work. The field-induced magnetisation of hydrogenated La-Fe-Si under pressure previously was seen to exhibit multiple steps, confirming Kuz'min and Richter's predictions. It may be interesting to investigate this property in the undoped compound to eliminate the possibility of pressure-induced hydrogen segregation. Spontaneous hydrogen segregation is known to occur in materials with a smaller hydrogen content than the empirical maximum.[40–43]

The derivative of $\Delta F(M)$ is also shown in Fig. 3; local minima in the free energy function are where $d\Delta f/dM = 0$. We may conclude that full doping of any of the four interstitials studied removes the shallow double-well potential, resulting in only a single well. This corresponds to the disappearance of the first order metamagnetic transition, as found experimentally for B, C, and N doping. We note that boron addition is detrimental to the total magnetisation as the minimum in $\Delta F(M)$ occurs at a lower value of M than for any other dopant. Of all the interstitials studied, hydrogen alters the double well picture the least. The shallow landscape of $\Delta F(M)$ takes on a concave curvature in the range of $M = 7 - 9\mu_B$ at full doping. The intrinsically small energy barrier for the parent compound and the hydrogen-doped material makes these compositions particularly sensitive to external parameters such as magnetic field, pressure and temperature and renders the first order IEM transition quasi-reversible.

Fig. 3b also reveals the sensitive nature of the metamagnetic states to the lattice parameters. An increase of about 0.5% in the lattice parameter upon H-doping generates a ground state with a high-spin configuration. In order to separate the changes in the magnetic state caused by the volume expansion (chemical pressure) due to the inclusion of large interstitials such as nitrogen from those caused by additional valence electrons, we also carried out calculations with empty spheres (Es) included at the 24*d* crystallographic site. For a direct comparison,

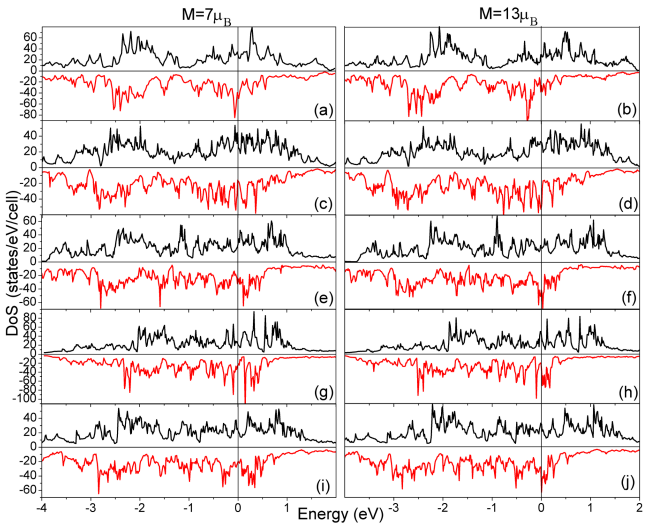

Figure 4: Up- and down DOS for $LaSiFe_{12}$ (i, j), $LaSiFe_{12}Es_3$ (g, h), $LaSiFe_{12}H_3$ (e, f), $LaSiFe_{12}N_3$ (c, d) and $LaSiFe_{12}B_3$ (a, b) at M=7μ_B (left column) and 13μ_B (right column) as calculated by FSM.

the same lattice constant was adopted for both Z = N and Es.

To further examine the appearance of a metastable low-spin state at around $M = 7\mu_B$ and the emergence of an energy barrier near $M = 13\mu_B$, DOS calculations were performed with fixed spin moments at these two values of magnetisation for each system. The results are shown in Fig. 4. For both X=H and Es, the Fermi level is located in a deep valley for both the minority and majority-spin DOS at M=7μ_B, similar to that found in the parent alloy. This well-defined valley in the DOS is destroyed for X = B and N. By contrast, the electronic features found in the DOS for M=13μ_B differ significantly; high peaks in the DOS appears at E_F for both minority and majority-spin states for the undoped as well as for Z=H and Es alloys, whilst only a moderate peak in height for Z=N and B are observed. It is thus apparent that the valleys and peaks around E_F can be attributed to the low-spin state and the energy barrier in $\Delta F(M)$.

In Fig. 5, we show the electronic band structure calculated for $M = 13\mu_B$, in order to provide an explanation for the above peaks in the electronic DOS. We note that a 0.01 eV offset was added to the energy level of p bands of N for clarity in the figure. We may make several qualitative observations. First, the flat and quasi-degenerate t_{2g} and e_g bands are widely observed toward representative k-directions along the Brillouin zone in the parent alloy. The additional charge supplied by the H atoms shifts the position of the Fermi level upwards but the character of these 3d bands is conserved. Second, in the empty sphere configuration (Z=Es), where the significantly larger lattice structure of the nitrogenated alloy is adopted without any addition of charge, strong narrowing of the bandwidth is found but the dispersion of each

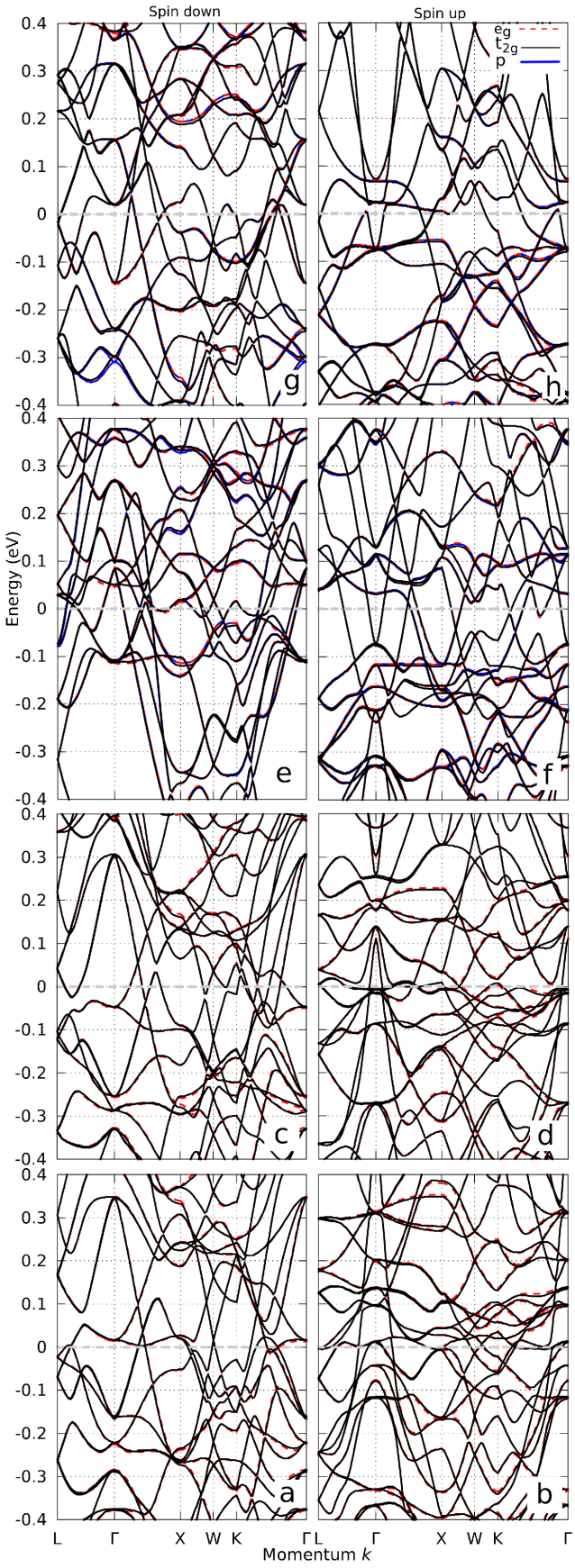

Figure 5: Up- and down spin band dispersions for $LaSiFe_{12}$ (a,b), $LaSiFe_{12}H_3$ (c,d) and for $LaSiFe_{12}N_3$ (e,f) and $LaSiFe_{12}B_3$ (g,h) at M=13μ_B as calculated by FSM.

band is once again preserved (not shown).

Third, the situation is very different for both Z=N and B, as the band structure is strongly altered at full doping. For Z=B, strong $p-d$ band mixing occurs between -0.3 and -0.6 eV for the majority spin states in all k-directions. In addition, broad bands originating from the p-states of boron appear at the Γ point about -0.3 eV for the minority spins. The formation of these hybrid $p-d$ bands ultimately results in the vanishing of the well-formed peak and valley structures of the DOS around E_F as shown in Fig. 4 and in Fig. 2. Finally, for nitrogen doping most of the flat bands appear just above E_F, apart from some minor ones around -0.5 eV in the W direction for the minority spins. Here, the $p-d$ mixing occurs mainly between bands in the K and W directions. Bands of e_g character show especially pronounced mixing with p-electrons. The number of flat bands around E_F is decreased as compared to the undoped system and as a result the DOS has uneven features with small peaks that are detrimental to the IEM. transition.

IV. CONCLUSIONS

We have investigated the effect of selected s- and p-block interstitial elements on the electronic, lattice and magnetic properties of $La(Fe,Si)_{13}$ using DFT. Our calculations find that a good correlation between the expansion of the unit cell and the size of the dopant. Fixed spin moment calculations yield a double well structure in the free energy of $LaFe_{12}Si$ as a function of magnetisation, which may be seen as the basis of the itinerant electron metamagnetic transition. Significantly, hydrogenation alters the electronic and magnetic structure of $LaSiFe_{12}$ to a much smaller degree than B, C and N dopants. This means that the first order IEM is much more robust to H insertion than to interstitial B, C, or N.

An analysis of the projected electronic DOS reveals that the dominant electronic states related to hydrogen insertion appear at around -8 to -7 eV, where very little contribution from Fe, Si and La elements is present. The additional charge of the hydrogen atoms elevates the Fermi level but the character of the bands is unaltered. The latter feature is also evident in the empty sphere configuration, where the nitrogenated lattice parameters are simulated without the N inclusions; only a narrowing of the band-width is found but the dispersion of each band remains mostly unaffected.

Consequently, hydrogen provides perhaps the only chemical pressure on the lattice that avoids significant alterations to the electronic structure of $LaSiFe_{12}$. In the case of the other dopants (B, C, N) broad bands originating from their p-states appear at energy levels, where the $3d$ states of Fe are also present. The formation of these hybrid $p-d$ bands results in the disappearance of the peak and valley structures in the electronic DOS around E_F, thereby reshaping the shallow free energy landscape and ultimately destroying the first order IEM of $LaSiFe_{12}$.

Acknowledgments

The research leading to these results has received funding from the European Community's 7th Framework Programme under Grant Agreement No. 310748 "DREAM". Computing resources provided by Darwin HPC and Camgrid facilities at The University of Cambridge and the HPC Service at Imperial College London are also gratefully acknowledged.

[1] P. Weiss and A. Piccard, J. Phys. (Paris) **5th Ser.**, 103 (1917).
[2] A. Smith, The European Physical Journal H **38**, 507 (2013).
[3] W. F. Giauque and D. P. MacDougall, Phys. Rev. **43**, 768 (1933).
[4] P. Debye, Annalen der Physik **386**, 1154 (1926).
[5] W. F. Giauque, Journal of the American Chemical Society **49**, 1864 (1927).
[6] V. K. Pecharsky and K. A. Gschneidner, Jr., Phys. Rev. Lett. **78**, 4494 (1997).
[7] G. V. Brown, Journal of Applied Physics **47**, 3673 (1976).
[8] K. G. Sandeman, Scripta Materialia **67**, 566 (2012).
[9] I. D. Hughes, M. Dane, A. Ernst, W. Hergert, M. Luders, J. Poulter, J. B. Staunton, A. Svane, Z. Szotek, and W. M. Temmerman, Nature **446**, 650 (2007).
[10] M.-H. Phan and S.-C. Yu, Journal of Magnetism and Magnetic Materials **308**, 325 (2007).
[11] Z. Gercsi and K. G. Sandeman, Phys. Rev. B **81**, 224426 (2010).
[12] Z. Gercsi, K. Hono, and K. G. Sandeman, Phys. Rev. B **83**, 174403 (2011).
[13] J. B. Staunton, M. dos Santos Dias, J. Peace, Z. Gercsi, and K. G. Sandeman, Phys. Rev. B **87**, 060404 (2013).
[14] A. Barcza, Z. Gercsi, K. S. Knight, and K. G. Sandeman, Phys. Rev. Lett. **104**, 247202 (2010).
[15] H. Yamada and K. Terao, Phase Transitions **75**, 231 (2002).
[16] N. H. Dung, Z. Q. Ou, L. Caron, L. Zhang, D. T. C. Thanh, G. A. de Wijs, R. A. de Groot, K. H. J. Buschow, and E. Brück, Advanced Energy Materials **1**, 1215 (2011).
[17] E. K. Delczeg-Czirjak, L. Delczeg, M. P. J. Punkkinen, B. Johansson, O. Eriksson, and L. Vitos, Phys. Rev. B **82**, 085103 (2010).
[18] E. K. Delczeg-Czirjak, L. Bergqvist, O. Eriksson, Z. Gercsi, P. Nordblad, L. Szunyogh, B. Johansson, and L. Vitos, Phys. Rev. B **86**, 045126 (2012).
[19] Z. Gercsi, E. K. Delczeg-Czirjak, L. Vitos, A. S. Wills, A. Daoud-Aladine, and K. G. Sandeman, Phys. Rev. B **88**, 024417 (2013).

[20] X. Liu, J. P. Liu, Q. Zhang, and Z. Altounian, Physics Letters A **377**, 731 (2013).
[21] P. I. Krypiakewytsch, O. S. Zaretschniuk, E. I. Hladyschewskyj, and O. I. Bodak, Z. anorg. allg. Chem. **358**, 90 (1968).
[22] H. Yamada, Phys. Rev. B **47**, 11211 (1993).
[23] A. Fujita, Y. Akamatsu, and K. Fukamichi, Journal of Applied Physics **85**, 4756 (1999).
[24] G. J. Wang, F. Wang, N. L. Di, B. G. Shen, and Z. H. Cheng, Journal of Magnetism and Magnetic Materials **303**, 84 (2006).
[25] X. B. Liu and Z. Altounian, Journal of Magnetism and Magnetic Materials **264**, 209 (2003).
[26] M. D. Kuz'min and M. Richter, Phys. Rev. B **76**, 092401 (2007).
[27] A. Fujita and H. Yako, Scripta Materialia **67**, 578 (2012).
[28] G. Kresse and J. Furthmuller, Phys. Rev. B **54**, 11169 (1996).
[29] J. P. Perdew, K. Burke, and M. Ernzerhof, Phys. Rev. Lett. **77**, 3865 (1996).
[30] S. H. Vosko, L. Wilk, and M. Nusair, Canadian Journal of Physics **58**, 1200 (1980).
[31] M.-K. Han and G. J. Miller, Inorganic Chemistry **47**, 515 (2008).
[32] F. Wang, G. J. Wang, F. X. Hu, A. Kurbakov, B. G. Shen, and Z. H. Cheng, Journal of Physics: Condensed Matter **15**, 5269 (2003).
[33] M. Rosca, M. Balli, D. Fruchart, D. Gignoux, E. Hlil, S. Miraglia, B. Ouladdiaf, and P. Wolfers, Journal of Alloys and Compounds **490**, 50 (2010).
[34] H. Hamdeh, H. Al-Ghanem, W. Hikal, S. Taher, J. Ho, D. Anh, N. Thuy, N. Duc, and P. Thang, Journal of Magnetism and Magnetic Materials **269**, 404 (2004).
[35] O. K. Andersen and O. Jepsen, Phys. Rev. Lett. **53**, 2571 (1984).
[36] O. Jepsen and O. K. Andersen, The Stuttgart TB-LMTO-ASA Program version 47, MPI fur Festkuorperforschung, Stuttgart, Germany. 2000.
[37] The implementation of the fixed spin moment method was provided by I. I. Mazin.
[38] L. Jia, J. Sun, J. Shen, B. Gao, T. Zhao, H. Zhang, F. Hu, and B. Shen, Journal of Alloys and Compounds **509**, 5804 (2011).
[39] H. Zhang, F. X. Hu, J. R. Sun, and B. G. Shen, Science China Physics, Mechanics and Astronomy **56**, 2302 (2013).
[40] A. Barcza, M. Katter, V. Zellmann, S. Russek, S. Jacobs, and C. Zimm, IEEE Transactions on Magnetics **47**, 3391 (2011).
[41] M. Krautz, J. D. Moore, K. P. Skokov, J. Liu, C. S. Teixeira, R. Schäfer, L. Schultz, and O. Gutfleisch, Journal of Applied Physics **112**, 083918 (2012).
[42] C. B. Zimm and S. A. Jacobs, Journal of Applied Physics **113**, 17A908 (2013).
[43] O. L. Baumfeld, Z. Gercsi, M. Krautz, O. Gutfleisch, and K. G. Sandeman, Journal of Applied Physics **115**, 203905 (2014).